Non ideal iris recognition based elastic snakes and graph matching model

Nouf Saeed Al Otaibi

***Abstract*— normally, iris recognition technologies robustly identify a person from its iris patterns, but they perform under a constrained environment to acquire good quality image data. In this paper, we have enhanced Elastic Graph Matching to the Modified EGM (M-EGM), which is afford to handle misalignments between irises by enhancing the robustness of node descriptors and cost function. The improved performance of the M-EGM was evaluated through the recognition simulation based on arbitrary irises. Individual segmented irises are represented as a labeled graphs. Nodes are labeled with robust jets; edges are labeled with distance vectors. The improved cost function is defined to compare two irises graph, taking into account the similarities of individual robust jets and the relative distortion of the graphs. Recognition results are given for galleries of irises from CASIA version 1 and UBIRIS databases. The numerical results show that, the M-EGM is an effective in the presence of partial occlusion as well as for iris matching process. We also compare our results with previous results and find out that, the M-EGM is an effective matching performance.**

***Index Terms*— Iris recognition, segmentation, modified elastic graph matching, feature extraction, Gabor wavelets**

I. INTRODUCTION

The generalized elastic graph matching is discussed for face recognition in [1]. Elastic graph matching is a popular technique in face recognition field for the robust face recognition to a rotation in depth and facial features, and is presented for iris recognition in [2]. Biometrics is considered a more capable technique to establish exactly a person's identity by his own behavioral or physiological characteristics. Special features are used for personnel recognition by current biometric applications include retina, iris, palm-prints, facial features, handwriting signature, gait, DNA, fingerprints [3, 4].

The human iris is a circular segment between sclera and pupil and its complex pattern contains many different features such as furrows, crypts, corona, arching ligaments, ridges and freckles. The iris is preserved from the external medium behind the eyelids and cornea. The radial features of the iris stay stable and fixed from about one year of age throughout one's life. The unique characteristics of the iris led to the evolution of the use of biotechnology in the identification of people through it and opened the door to researchers in the field of security to develop many different methods and algorithms to develop them. Many researchers have used the iris to identify people [5-9].

Despite the characteristics of the iris, which cannot be repeated for more than one person and although it has been applied in most airports in the world and places of entry security and border, but it occupies the attention of a large number of researchers in the security field to obtain the best possible results and avoid the problems of the matching process. In the past few years, some methods made certain improvement based on the Daugman's method.

Although the iris has received considerable attention in recent years, it remains the focus of many researchers. For example, the principle of dictionaries learning for iris recognition is discussed in [10]. Given the importance of the iris of the eye was the work of a comprehensive review of the installation of the iris and secrets to enable researchers to use has been discussed in [11]. The effect of using pre-compressed data in iris segmentation and reform the connection between iris segmentation execution and general image quality metrics is presented in [12]. The sparse representation coding followed by spatial pyramid mapping method for feature computation from iris pattern is shown in [13]. The problem of finding the accurate position of an eye for mobile iris recognition system which is crucial is presented in [14]. Non-ideal iris localization schemes using near infrared illumination, visible wavelength illumination images contain noise such as non-uniform illumination, defocus, etc. is presented in [15]. A bio-orthogonal wavelet based iris recognition system, which modified and demonstrated to perform off-angle iris recognition is discussed in [16]. An efficient and robust segmentation of noisy iris images for non-cooperative iris recognition is described in [17]. Iris image segmentation and sub-optimal images is discussed [18]. Comparison and combination of iris matchers for reliable personal authentication are introduced [19]. Noisy iris segmentation, with boundary regularization and reflections removal, is discussed [20]. Iris representation based on binary features of the multi-scale Taylor expansion is discussed by [21]. A non-ideal iris image segmentation approach based on graph cut is presented that uses both the appearance and eye geometry information [22]. The changes in iris texture with time, like disease and medication are discussed in [23]. In view of the limitation of poor direction selectivity about the 2-D wavelet transform and the problem of redundancy on contour let transform, an iris texture feature extraction method based on wavelet-based contourlets transform for obtaining high quality features is proposed in [24].

II. OUTLINE

The rest of this paper is organized as following, we have introduced the iris segmentation process based on Hough transform which is a critical to the success of any iris recognition system. To remove the noisy from the segmented iris region, we have applied a smoothing filter to delay the noise. The next step we have demonstrated how we have selected the inside iris node to present each iris image as a

Nouf Saeed Al Otaibi, Computer Science Department, Shaqra University

graph and extract an invariant Gabor feature vector at each node. The similarity between correspondence nodes is computed and low similarity is dropped from graph matching. Finally we have displayed the numerical results.

III. IRIS SEGMENTATION

The phase of iris separation from the eyelashes and eyelid is one of the most important stages in the iris recognition system. The iris segmentation process has implemented by the following core steps. Locating the radius and center of the iris in the input image by using

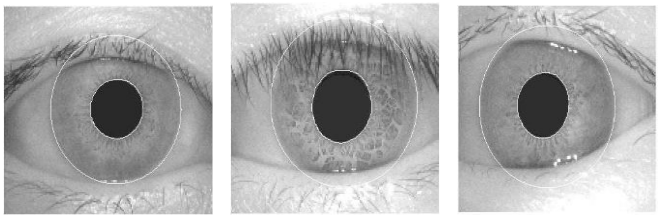

(a) (b) (c)

Fig 1: Errors in pupil localization by using the circular Hough transform.

Daugman technique [7]. Then we define a set of points that determine the pupil configuration and near the center of the iris. Finally, we define the boundaries of the pupil points by using the snakes. The pseudo code is demonstrated in table 1.

Assuming a circle with the center (i_c, j_c) and radius r, the edge points that are located over the circle result in a zero value of the function g. The value of g is then transformed to 1 by the h function, which represents the local pattern of the contour. The local patterns are then used in a voting procedure using the Hough transform, in order to locate the proper pupil and limbus boundaries. In order to detect limbus, only vertical edge information is used. The upper and lower parts, which have the horizontal edge information, are usually covered by the two eyelids. The horizontal edge information is used for detecting the upper and lower eyelids, which are modeled as parabolic arcs.

Table 1: The pseudo code of Hough transform

Read image $I(i, j), \quad 1 < i, j < N$

Apply a smoothing filter

$$I_E = -\left|G_\sigma(i,j) * \nabla^2 I(i,j)\right|^2,$$

$$G_\sigma(i,j) = \frac{1}{2\pi\sigma^2}\exp-\left(\frac{(i-i_0)^2+(j-j_0)^2}{2\sigma^2}\right),$$

Find edge in the input image

Find all points $(i_x, j_y), \quad x, y = 1,2,...,n$

and (i_c, j_c) and satisfy the following

$$T(i_c, j_c, r) = \sum_1^n t(i_x, j_y, i_c, j_c, r),$$

$$t(i_x, j_y, i_c, j_c, r) = \begin{cases} 1 & if\ g(i_x, j_y, i_c, j_c, r) = 0 \\ 0 & \text{otherwise} \end{cases},$$

$$g(i_x, j_y, i_c, j_c, r) = (i_x - i_c)^2 + (j_y - j_c)^2 - r^2$$

3.1 Elastic snake model

To localize the pupil in eye image, we have used elastic snake models. Snake model respond to pre-set internal and external forces by deforming internally or moving across an image until equilibrium is reached. The snake contains a number of vertices, whose positions are changed by two opposing forces, an internal force, which is

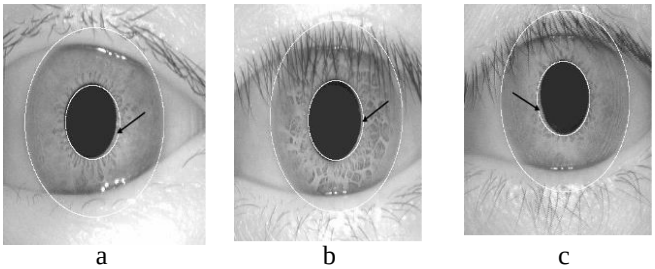

a b c

Fig. 2: Segmentation of a sub-optimal iris image: (a) the original iris image, (b) the final segmentation.

dependent on the desired characteristics, and an external force, which is dependent on the image. Each vertex is moved between time *t* and *t + 1* by

$$V_i(t+1) = V_i(t) + \beta F_{\text{int},i}(t) + (1-\beta)F_{ext,i}(t), \qquad (1)$$

Where $F_{\text{int},i}$ is the internal force, $F_{ext,i}$ is the external force and V_i is the position of vertex *i*. For localization of the pupil region, the internal forces are calibrated so that the contour forms a globally expanding discrete circle. The external forces are usually found using the edge information. In order to improve accuracy, we have used the variance image, rather than the edge image. A point interior to the pupil is located from a variance image and then a discrete circular active contour (DCAC) is created with this point as its center. The DCAC is then moved under the influence of internal and external forces until it reaches equilibrium, and the pupil is localized. The internal forces are responsible to expand the contour into a perfect polygon with a radius σ larger than the contour average radius. The internal force $F_{\text{int},i}$ applied to each vertex, V_i is defined as

$$F_{\text{int},i} = \overline{V_i} - V_i \qquad (2)$$

Where $\overline{V_i}$ is the expected position of the vertex in the perfect polygon. The position of $\overline{V_i}$ can be obtained with respect to C_r, the average radius of the current contour, and the contour center, $C = (C_x, C_y)$. The center of a contour which is the average position of all contour vertices is defined as

$$C = (C_x, C_y) = \frac{1}{n}\sum_{i=1}^{n} V_i \qquad (3)$$

The average radius of the contour is the average distance of all the vertices from the defined center point C_r is as the following equations

$$C_r = \frac{1}{n}\sum_{i=1}^{n} \|V_i - C\| \qquad (4)$$

Then the position of the vertices of the expected perfect polygon is obtained as

$$\overline{V_i} = (C_x + (C_r + \delta)\cos(2\pi i / n), \; C_y + (C_r + \delta)\cos(2\pi i / n)) \quad (5)$$

Where n is the total number of vertices. The internal forces are designed to expand the contour and keep it circular. The force model assumes that pupil and limbus are globally circular, rather than locally, to minimize the undesired deformations due to specular reflections and dark patches near the pupil boundary. The contour detection process of the model is based on the equilibrium of the defined internal forces with the external forces. The external forces are obtained from the grey level intensity values of the image and are designed to push the vertices inward. The magnitude of the external forces is defined as:

$$\left\|F_{ext,i}\right\| = I(V_i) - I(V_i + \hat{F}_{ext,i}) \quad (6)$$

Where $I(V_i)$ is the grey level value of the nearest neighbor to V_i. $\hat{F}_{ext,i}$ is the direction of the external force for each vertex and it is defined as a unit vector given by:

$$\hat{F}_{ext,i} = \frac{C - V_i}{\|C - V_i\|} \quad (7)$$

Therefore, the external force over each vertex can be written as:

$$F_{ext,i} = \left\|F_{ext,i}\right\| \hat{F}_{ext,i} \quad (8)$$

The movement of the contour is based on the composition of the internal and external forces over the contour vertices. Replacement of each vertex is obtained iteratively by:

$$V_i(t+1) = V_i(t) + \beta F_{int,i}(t) + (1-\beta) F_{ext,i}(t) \quad (9)$$

Where β is a defined weight that controls the pace of the contour movement and sets the equilibrium condition of internal and external forces. The final equilibrium is achieved when the average radius and center of the contour becomes the same for the first time in m iterations ago. The discrete circular active contour is applied on the three images in Figure 3.

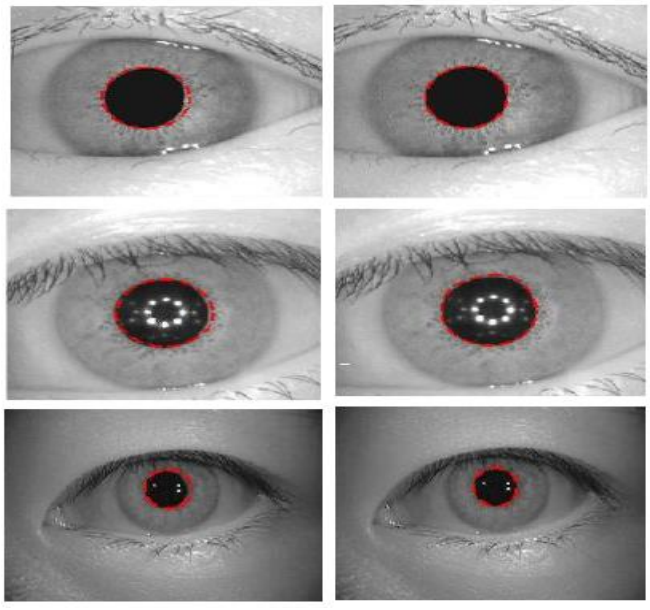

Figure 3: The segmentation of the DCA

3.2 Detecting eyelids, Eyelashes and noise regions

Detecting eyelashes requires proper choice of features and classification procedure due to complexity and randomness of the patterns. The proposed eyelash detection by Kong and Zhang (2010) consider eyelashes as two groups of separable eyelashes, which are isolated in the image, and multiple eyelashes, which are bunched together and overlap in the eye and applies two different feature extraction methods to detect eyelashes. Separable eyelashes are detected using 1-D Gabor filter, since the convolution of a separable eyelash with the Gaussian smoothing function results in a low output value. Thus, if a resultant point is smaller than a threshold, it is noted that this point belongs to an eyelash. Multiple eyelashes are detected using the variance of intensity. If the variance of intensity values in a small window is lower than a threshold, the center of the window is considered as a point in an eyelash. The two features combined with a connectivity criterion would lead to the decision of presence of eyelashes. In addition, an eyelash detection method is also proposed by Huang et al. that uses the edge information obtained by phase congruency of a bank of Log-Gabor filters. The edge information is also infused with the region information to localize the noise regions Fig. 4.

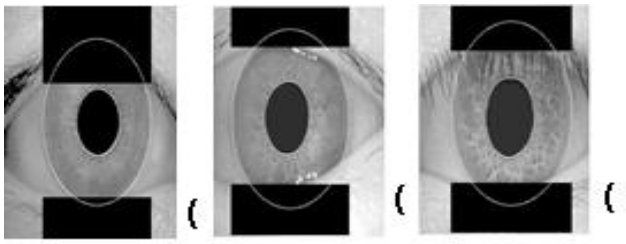

Fig. 4: The iris localization, where black regions denote detected eyelids and eyelashes regions.

IV. ROBUST GRAPH MATCHING

Let $I(i, j)$ be the gray level distribution of the input segmented iris image Fig. 4. Our image representation is based on the complex convolution. The segmented iris image $I(i, j)$ is presented as a features vector image; each point $\vec{x}_0 = (i_0, j_0)$ in the feature image is represented as a vector (jet) of Gabor wavelet coefficients calculated by convolution between $I(i, j)$ and Gabor kernels $\Phi_{\vec{k}}(\vec{x})$ by the following formula:

$$\Upsilon_{\mu,\nu} = \Upsilon(\vec{k}, \vec{x}_0) = I(\vec{x}_0) * \Phi_{\vec{k}}(\vec{x} - \vec{x}_0) \quad (10)$$

Which are parameterized by the two-dimensional vector and define by the equation:

$$\vec{k}_{\nu\mu} = \begin{pmatrix} k_\nu \cos\varphi_\mu \\ k_\nu \sin\varphi_\mu \end{pmatrix}, \quad k_\nu = \pi 2^{-\frac{\nu+2}{2}}, \; \varphi_\mu = \frac{\pi\mu}{8}, \quad (11)$$

$$\nu \in \{0,1,..., M\text{-}1\}, \; \mu \in \{0,...,L\text{-}1\}.$$

Gabor kernels $\Phi_{\vec{k}}(\vec{x})$ (Fig. 5) are given by the formula:

$$\Phi_{\vec{k}}(\vec{x}) = \frac{\vec{k}^2}{\sigma^2}\left(-\frac{\vec{k}^2\vec{x}^2}{2\sigma^2}\right)\left[e^{i\vec{k}\vec{x}} - e^{\frac{\sigma^2}{2}}\right] \quad (12)$$

To generate a robust jet, extracted Gabor wavelet coefficients are aligned as LxM Gabor wavelets coefficients matrix eq. (9).

$$A = \begin{bmatrix} \Upsilon_{0,0} & \dots & \Upsilon_{0,M-1} \\ \dots & \dots & \dots \\ \Upsilon_{L-1,0} & \dots & \Upsilon_{L-1,M-1} \end{bmatrix} = \left[\Upsilon_{\mu,\nu}\right]_{\substack{\mu=0,\dots,L-1 \\ \nu=0,\dots,M-1}} \quad (13)$$

Then we compute 2D Discrete Fourier Transform (DFT) of Gabor matrix Φ to get the form

$$\Omega = 2D\,DFT_{\mathrm{LxM}}(A) = \left[c_{\mu,\nu}\right]_{\substack{\mu=0,\dots,L-1 \\ \nu=0,\dots,M-1}} \quad (14)$$

We define our robust jet at $\vec{x}_0$ as a vector of aligned magnitude parts of elements of Ω.

$$\Upsilon_r(\vec{x}_0) = \left(|c_{0,0}|, |c_{1,0}|, \dots, |c_{L-1,M-1}|\right)/\rho \quad (15)$$

Where $\rho = \left(\sum_{\mu=0}^{L-1}\sum_{\nu=0}^{M-1}\left(|c_{\mu,\nu}|^2\right)\right)^{1/2}$

3.1 Robust cost function

Due to phase rotation, jets taken from image points only a few pixels apart from each other have very different coefficients, although representing almost the same local feature. This can cause severe problems for matching. Using phase has two potential advantages. Firstly, phase information is required to discriminate between patterns with similar magnitudes, should they occur, and secondly, since phase varies so quickly with location, it provides a means for accurate jet localization in an image. Assuming that two robust jets Υ_r and Υ'_r refer to object locations with small relative displacement $\vec{d}$, the phase shifts can be approximately compensated for by the terms $\vec{d}\vec{k}_j$, leading to a phase-sensitive similarity function

$$S_{ph}(\Upsilon_r, \Upsilon'_r) = \frac{\sum_j \lambda_j \lambda'_j \cos(\theta_j - \theta'_j - \vec{d}\vec{k}_j)}{\sqrt{\sum_j \lambda_j^2 \sum_j \lambda_j'^2}} \quad (16)$$

To compute it, the displacement $\vec{d}$ has to be estimated. This can be done by maximizing S_{ph} in its Taylor expansion explained in Wiskott 1997. It is actually a great advantage of this second similarity function that it yields this displacement information.

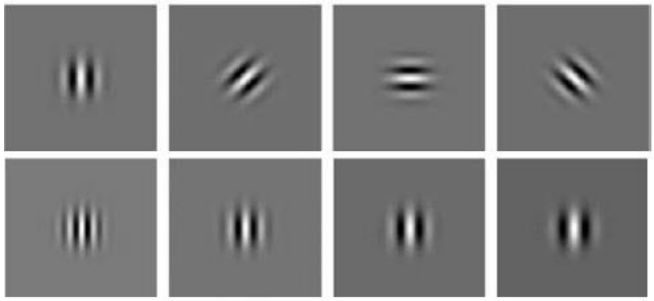

Fig. 5: Shows in the first row variation in orientation, second row variation in wavelength.

4.2 Matching

When matching a template (the input iris graph) M_T against the graphs of iris in database M_I, replica of its set of node positions $\{\vec{x}_c^{M_T}\}$ is placed in the image, or the corresponding image graph M_I creating the set of points $\{\vec{x}_c^{I}\}$, where $\vec{x}_i^{I} = \vec{x}_i^{M} + \vec{x}^{s}$ with an offset vector $\vec{x}^{s}$ common to all nodes. The graph formed by the set of points $\{\vec{x}_i^{I}\}$ is called the image graph. The template graph M_T is compared to the image graph M_I with offset $\vec{x}^{s}$ in terms of the cost function

$$S(M_T, M_I) = \frac{1}{N_V}\sum_{i\in V} S_{ph}(\Upsilon_{ir}^{I}, \Upsilon_{ir}'^{M}), \quad (17)$$

Where Υ_{rj}^{I} is the image jet taken at position $\{\vec{x}_i^{I}\}$, V is the set of visible nodes and N_V is their number. Now, the matching cost (17) is minimized by varying $\vec{x}^{s}$. First, the offset is taken through all points on a square grid with spacing of five pixels for which the replica of the model graph lies entirely within the image. Around the lattice point with minimal cost a better minimum is then found for a finer lattice with spacing 1. When an iris is occluded to a large eyelid and eyelash region, the total cost of its match is degraded by the many nodes that come to fall out the iris region and that correspondingly have low average similarity values. It is decided that this correct match cannot be outdone by a false match in some region of the image picked such that many nodes have above average similarity. The result of matching is illustrated in Fig. 6

V. Result and Discussion

To evaluate the effectiveness and the performance of the proposed method for iris recognition, we have used the CASIA version 1 and UBIRIS databases as the test and train dataset. The experiments are conducted in two modes: verification and identification. In the verification mode, the Receiver Operating Characteristic (ROC) curve depicts the relationship of False Accept Rate (FAR) versus False Reject Rate (FRR) (see Fig. 7). The area under the ROC curve

(denoted as AZ) reflects how well the intra-class and extra-class distributions can be distinguished and the ranges are from 0.5 to 1. For an ideal ROC curve, the value of AZ should be 1. It denotes that the intra and extra-class are inseparable while the AZ value is equal to 0.5.

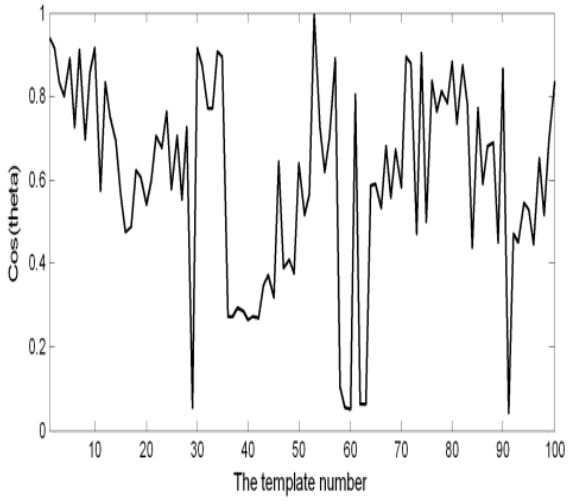

Fig. 6: The matching of the template graph of an image in CASIA against 100 stored model graph

Hence, the ROC curve is suitable for measuring the accuracy of the matching process and showing the achieved performance of a recognition algorithm. FAR is the probability of accepting an imposter as an authorized subject and FRR is the probability of a genuine authorized subject that is rejected as being an imposter. In the recognition mode, the Correct Recognition Rate (CRR) is adopted to assess the efficacy of the algorithm, as shown in Table 2.

Matching measure	Correct recognition rate (CRR) %
2D Gabor filter Daugman, 1993	99.3
Elastic Graph Match Farouk, 2011	98.5
Proposed M-EGM	98.8

Table 2: The correct recognition rates achieved by four matching measures using the CASIA and UBIRIS database. To assess the accuracy of the proposed algorithm, each test iris image in the database is individually matched to all the other iris images in the trained database. In the UBIRIS database, the total number of comparisons is 324351 where the numbers of intra-class and extra-class comparisons are 1792 and 322559 respectively. The EGM was tested by using 996 and 723 iris images from the CASIA and UBIRIS database respectively. The ROC curve (see Fig. 8) for the False Match Rate (FMR) and False Non-Match Rate (FNMR) are estimated. The ERM was found to give good correct recognition rates compared to other matching methods as shown in Table 2. The result of matching is illustrated in Fig. 8.

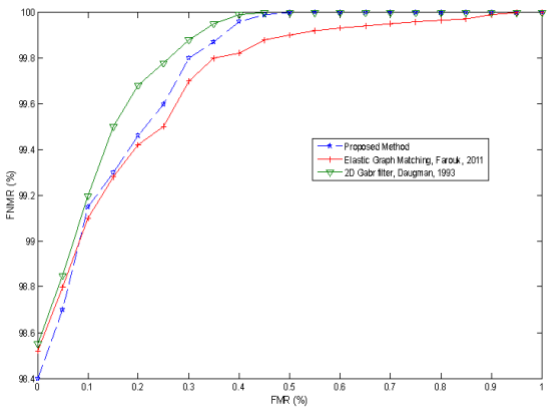

Fig. 7. Shows the ROC curves of the elastic graph matching with CASIA and UBIRIS databases.

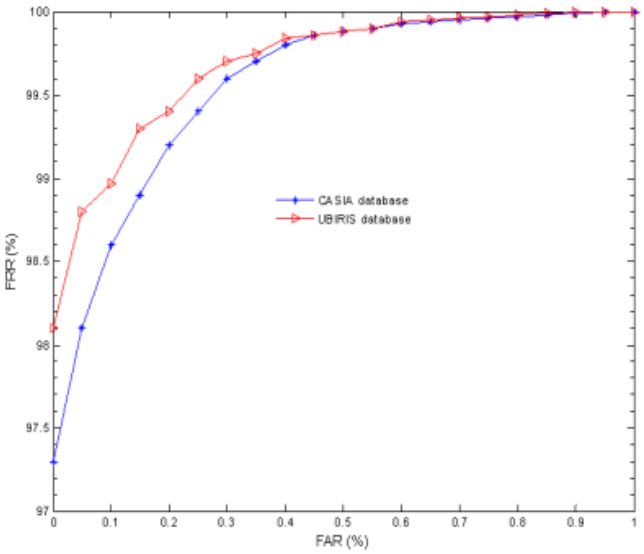

Fig. 8. The obtained ROC curves after applying different methods on UBIRIS database.

6. Conclusion

Here we have introduced a modified elastic graph matching technique for non-ideal iris recognition system. Also, we have treated the problem of nodes located on the boundary of the iris. Modified EGM technique is tested for iris recognition. Experimental results have shown that ignoring the boundary effect still can indicate eminent performance for iris recognition. All recognition rates are more than 95%. Therefore, the EGM method has demonstrated to be promising for iris recognition and is suitable for matching process. In future work, we will improve the processing method for iris templates to reduce the influence from light, eyelid, and eyelash.

REFERENCES

[1] Shin H., Kim S., and Choi, H. Generalized elastic graph matching for face recognition, Pattern Recognition Letters 28, 1077–1082, (2007).
[2] Farouk R. M., Iris recognition based on elastic graph matching and Gabor wavelet, Computer Vision and Image Understanding, 115, 1239–1244, (2011).
[3] Bowyer, K. W., Hollingsworth, K., Patrick, J. F., Image understanding for iris biometrics: A survey, Computer Vision and Image Understanding, 110, 281-307, (2008).
[4] Duta, N., A survey of biometric technology based on hand shape, Pattern Recognition, 42, 2797-2806, (2009).

[5] Daugman, J.,Statistical Richness of Visual Phase Information: Update on Recognizing Persons by Iris Patterns, Int. Journal of Computer Vision, 45 (1), 25-38, (2001).
[6] Daugman, J., Demodulation by Complex-valued Wavelets for Stochastic Pattern Recognition, International Journal of Wavelets, Multi-resolution and Information Processing, Vol. 1(1), 1-17, (2003).
[7] Daugman, J., How Iris Recognition Works, IEEE Transactions on Circuits and Systems for Video Technology, Vol. 14(1), 21-30, (2004).
[8] Boles, W., Boashash, B., A Human Identification Technique Using Images of The Iris and Wavelet Transform, IEEE Transactions on Signal Processing, 46, 1185-1188, (1998).
[9] Huang, P. S., Chiang, C. S., Liang, J. R., Iris recognition using Fourier-wavelet features, Lecture Notes in Computer Science, 3546, 14–22, (2005).
[10] Naseem I., Aleem A., Tongeri R. and Bennamoun M., Iris recognition using class-specific dictionaries, Computer & electrical engineering, 62, 178-193, (2017).
[11] Nguyen K., Fookes C., Jillela R., Sridharan S. and Ross A., Long range iris recognition: A survey, pattern recognition, 72, 123-143, (2017).
[12] Bergmueller T., Fehrenbach K., Schoell M. and Uhl A., Recompression effects in iris recognition, Image and vision computing, 58, 142-157, (2017).
[13] Umer S., Dhara, B. and Chanda B., Anovel cancelable iris recognition system based on feature learning techniques, Information sciences, 406-407, 102-118, (2017).
[14] Jung Y., Kim D., Son B. and Kim J., An eye detection method robust to eyeglasses for mobile iris recognition, Expert system with applications, 67,178-188, (2017).
[15] Jan F. Non-circular iris contours localization in the visible wavelength eye images, Computer & electrical engineering, 62, 166-177, (2017).
[16] Abhyankara, A., Schuckers, S., A novel bio-orthogonal wavelet network system for off-angle iris recognition, Pattern Recognition, 43, 987-1007, (2010).
[17] Tan, T., He, Z., Sun, Z., Efficient and robust segmentation of noisy iris images for non-cooperative iris recognition, Image and Vision Computing, 28, 223-230, (2010).
[18] Matey, J. R., Broussard, R., Kennell, L., Iris image segmentation and sub-optimal images, Image and Vision Computing, 28, 215-222, (2010).
[19] Kumar, A., Passi, A., Comparison and combination of iris matchers for reliable personal authentication, Pattern Recognition, 43, 1016-1026, (2010).
[20] Labati, R. D., Scott,i F., Noisy iris segmentation with boundary regularization and reflections removal, Image and Vision Computing, 28, 270-277, (2010).
[21] Algrids B., Justas K. and Volker K., Iris recognition by fusing different representations of multi-scale Taylor expansion, Computer Vision and Image Understanding, 115, 6, (2011), 804-816.
[22] Pundlik S., Woodard D., and Birchfield S., Iris segmentation in non-ideal images using graph cuts, Image and Vision Computing, 28, 12, 1671-1681, (2010).
[23] Rankin D. M., Scotney B.W., Morrow P.J., and Pierscionek B.K., Iris recognition failure over time: The effects of texture, Pattern Recognition, 45, 1, 145-150, (2012).
[24] Luo Z., Iris feature extraction and recognition based on wavelet Based contourlet transform, Procedia Engineering, 29, 3578 – 3582, (2012).